Mausam, (1979), **30**, 1, 69-78

551 : 55 : 551.510.42 : 628.5

Application of Pielke model to air quality studies

MURARI LAL*

Meteorological Office, Pune

(Received 14 February 1978)

ABSTRACT. In this paper an attempt has been made to evaluate the capability of University of Virginia's mesoscale (Pielke) model for air quality studies. The development of the physical equations and numerical techniques employed in the model are described and deficiencies indicated. It is demonstrated that, although the Pielke model has certain limitations for air quality purposes, it can still provide valuable qualitative understanding of ambient air quality for a limited range of conditions.

1. Introduction

The last decade has seen widespread concern regarding man's impact on the environment. Numerous indicators bear witness to severe inadvertent environmental effects. This concern is now embodied in legislation in several countries requiring assessment of envionmental impacts of proposed industrial projects and restricting emissions of air pollutants. Soundly based assessments can only be achieved, however, through understanding of physcial processes affecting air quality. Increasing sophistication of air-quality models has led to their general acceptance as valid techniques in air quality assessment.

Perhaps the best known model for mesoscale simulations is that of Mahrer and Pielke (1976). In this report, development of the governing equations and numerical techniques employed in the model are treated. Extensive test simulations of the model on a variety of simple cases, which give valuable insight into the sensitivity of the results, particularly to initialization and boundary conditions are discussed. Further, results from the model airflow predictions as applied to the calculation of air pollution trajectories for a sea breeze situation are reported. The importance to inland air quality of pollution sources along the shore for this idealized case is discussed.

2. The model equation

The model equations appear in various papers written during the period of development by Pielke. The earliest references describe the three-dimensional sea breeze model with the variables expressed as deviations from the synoptic scale state (Pielke 1973, 1974a). The equations for both two and three-dimensional versions are presented in Pielke (1974 b). Subsequently, significant changes were made in formulating the model equations. The dependent variables became the total quantities (perturbations *plus* large-scale values) rather than simply the perturbation. In addition, prognostic equation for the boundary layer height (attributed to Deardorff 1974) was added. These changes, along with the new two-dimensional model equations, were given in Pielke and Mahrer (1975). Later stages in model development included the incorporation of topography (with transformation to a terrain following coordinate system) in the two-dimensional model (Mahrer and Piekle 1975) and in the three-dimensional version (Mahrer and Pielke 1976).

A considerable amount of searching through the above-mentioned papers was done to obtain the latest version of the governing equations in their most general form. In Table 1, the model equations are presented in tabular form beginning with the most fundamental version. Subsequent tables concentrate on the governing equations of model after the incorporation of simplifying assumptions and approximations.

Tensor notation is used to express the equations using a minimum of effort. Unrepeated subscripts indicate free variables; the subscript is understood to be either 1, 2 or 3 and the corresponding variable is any of the three vector components or nine second-order tensor components, etc. For example :

$$x_i \equiv (x_1, x_2, x_3) \equiv (x, y, z)$$

$$u_i \equiv (u_1, u_2, u_3) \equiv (u, v, w)$$

$$u_i u_j \equiv (u^2, uv, uw, vu, v^2, vw, wu, wv, w^2)$$

*Present affiliation : Department of Geophysics, Banaras Hindu University, Varanasi.

TABLE 1

Fundamental governing equations

$$\frac{\partial u_i}{\partial t} = -u_j \frac{\partial u_i}{\partial x_j} - \frac{1}{\rho}\frac{\partial p}{\partial x_i} - g\,\delta_{3i} + \nu \frac{\partial^2 u_i}{\partial x_j\,\partial x_j} - \epsilon_{ijk} f_j u_k$$

$$\frac{\partial \theta}{\partial t} = -u_j \frac{\partial \theta}{\partial x_j} + \chi \frac{\partial^2 \theta}{\partial x_j \partial x_j} - \frac{1}{\rho C_p}\frac{\partial R_j}{\partial x_j} - \nabla \frac{L_v \theta}{C_p T}\left[\frac{d q_s}{d t}\right]$$

$$\frac{\partial q}{\partial t} = -u_j \frac{\partial q}{\partial x_j} + \chi \frac{\partial^2 q}{\partial x_j \partial x_j} + \Delta\left[\frac{d q_s}{d t}\right]$$

$$\frac{\partial u_j}{\partial x_j} = 0$$

Repeated subscript simplying the Einstein summation convention (unless otherwise indicated); the equivalent form in vector notation is the dot-product. Thus :

$$u_i\,u_i = u^2 + v^2 + w^2$$

$$u_j \frac{\partial}{\partial x_j} = u\frac{\partial}{\partial x} + v\frac{\partial}{\partial y} + w\frac{\partial}{\partial z}$$

Two important (and useful) tensors are δ_{ij} and ϵ_{ijk} (Kronecker's Delta and the Alternating unit tensor, respectively).

Table 1 shows the Navier-Stokes equations (the three component equations expressed as one equation in tensor form), thermodynamic equation, moisture conservation equation and mass conservation equation (or continuity equation). Similar notations are given in Monin and Yaglom (1971), Haltiner (1971) and Busch (1973).

The Navier-Stokes equations consist of terms representing advection/convection, acceleration due to pressure gradient, acceleration due to gravity, molecular viscous diffusion and coriolis effects, respectively. The thermodynamic and moisture conservation equations incorporate advection/convection, molecular conductivity/diffusivity, radiation flux divergence (in the thermodynamic equation only) and condensation/latent heat release respectively. The remaining partial differential equation is the "quasi-Boussinesq" form of the continuity equation.

As a preliminary simplification of these equations, molecular viscous/diffusion effects are assumed negligible in comparison with their eddy diffusive counterparts. The radiative flux divergence is not considered in the model at present although neglect of this physical effect may be questioned in many circumstances (Busch 1973). Condensation effects are also ignored since the condensation terms are only important when the air becomes saturated in a region of upward vertical motion.

As regard variations in the density and temperature fields, Busch (1973) considers deviations of these quantities from a reference state

TABLE 2

Mean Reynold's equations

$$\frac{\partial \bar{u}_i}{\partial t} = -\bar{u}_j \frac{\partial \bar{u}_i}{\partial x_j} - \bar{\theta}\frac{\partial \bar{\pi}}{\partial x_i} - g\,\delta_{3i} - \epsilon_{ijk} f_j \bar{u}_k - \frac{\partial}{\partial x_j}\left(\overline{u_i' u_j'}\right)$$

$$\frac{\partial \bar{\theta}}{\partial t} = -\bar{u}_j \frac{\partial \bar{\theta}}{\partial x_j} - \frac{\partial}{\partial x_j}\left(\overline{u_j\,\theta'}\right)$$

$$\frac{\partial \bar{q}}{\partial t} = -\bar{u}_j \frac{\partial \bar{q}}{\partial x_j} - \frac{\partial}{\partial x_j}\left(\overline{u_j'\,q'}\right)$$

$$\frac{\partial \bar{u}_j}{\partial x_j} = 0$$

which is hydrostatic, dry adiabatic and horizontally homogeneous. The same assumptions have been made in this model about deviation from a locally defined mean state.

For the derivation of Reynolds equations for the mean variables, it is assumed that

$$\left.\begin{aligned} u_i &= \bar{u}_i + u_i' \\ \theta &= \bar{\theta} + \theta' \\ q &= \bar{q} + q' \\ \pi &= \bar{\pi} + \pi' \end{aligned}\right\} \qquad (1)$$

where the mean of a perturbation is zero by definition. The additional turbulent flux divergence terms are also included in final forms shown in Table 2 which are generated by the non-linear advection/convection terms.

An examination of the vertical equation of motion reveals that for mid-latitudes, $f_j \approx 10^{-4}$ s^{-1}, whereas $g \approx 10$ m.s^{-2}. Thus, for wind speeds of the order of 10 m.s^{-1}, the coriolis term will be four orders of magnitude less than g and may be neglected. Haltiner (1971) shows by scale analysis of the vertical equation of motion that a sufficient condition for the hydrostatic approximation is :

$$D^2/L^2 << 1 \qquad (2)$$

TABLE 3

Final governing equations

$$\frac{\partial u}{\partial t} = -u_j \frac{\partial u}{\partial x_j} - \theta \frac{\partial \pi}{\partial x} + f_3 v - f_2 w + \frac{\partial}{\partial x}\left(K_H \frac{\partial u}{\partial x}\right) + \frac{\partial}{\partial y}\left(K_H \frac{\partial u}{\partial y}\right) + \frac{\partial}{\partial z}\left(K_H^{(m)} \frac{\partial u}{\partial z}\right)$$

$$\frac{\partial v}{\partial t} = -u_j \frac{\partial v}{\partial x_j} - \theta \frac{\partial \pi}{\partial y} - f_3 u + \frac{\partial}{\partial x}\left(K_H \frac{\partial v}{\partial x}\right) + \frac{\partial}{\partial y}\left(K_H \frac{\partial v}{\partial y}\right) + \frac{\partial}{\partial z}\left(K_H^{(m)} \frac{\partial v}{\partial z}\right)$$

$$\frac{\partial \pi}{\partial z} = -\frac{g}{\theta}$$

$$\frac{\partial \theta}{\partial t} = -u_j \frac{\partial \theta}{\partial x_j} + \frac{\partial}{\partial x}\left(K_H \frac{\partial \theta}{\partial x}\right) + \frac{\partial}{\partial y}\left(K_H \frac{\partial \theta}{\partial y}\right) + \frac{\partial}{\partial z}\left(K_z^{(\theta)} \frac{\partial \theta}{\partial z}\right)$$

$$\frac{\partial q}{\partial t} = -u_j \frac{\partial q}{\partial x_j} + \frac{\partial}{\partial x}\left(K_H \frac{\partial q}{\partial x}\right) + \frac{\partial}{\partial y}\left(K_H \frac{\partial q}{\partial y}\right) + \frac{\partial}{\partial z}\left(K_H^{(q)} \frac{\partial q}{\partial z}\right)$$

$$\frac{\partial w}{\partial z} = -\left(\frac{\partial u}{\partial x} + \frac{\partial v}{\partial y}\right)$$

where D is a characteristic vertical scale and L is a characteristic horizontal scale (roughly a quarter wavelength of the disturbances of interest). Assuming that the inequality (2) is satisfied, *i.e.*, the model is hydrostatic, all terms in the vertical equation of motion except the pressure gradient and gravitational terms become negligible by comparison.

The next problem is closure of the Reynold's equations. The nature of this problem is summarized concisely by Busch (1973). In Pielke model, first-order closure, specifically K-theory, has been invoked. It has been assumed that

$$-\overline{\tilde{u}_j' u_i'} = \begin{cases} K_H \dfrac{\partial \tilde{u}_i}{\partial x_j}, & j=1, 2 \\ K_z(m) \dfrac{\partial \tilde{u}_i}{\partial x_j}, & j=3 \end{cases}$$

$$-\overline{u_j' \theta'} = \begin{cases} K_H \dfrac{\partial \theta}{\partial x_j}, & j=1, 2 \\ K_z(\theta) \dfrac{\partial \theta}{\partial x_j}, & j=3 \end{cases} \qquad (3)$$

$$-\overline{u_j' q'} = \begin{cases} K_H \dfrac{\partial q}{\partial x_j}, & j=1, 2 \\ K_z(q) \dfrac{\partial q}{\partial x_j}, & j=3 \end{cases}$$

As a final step, the two horizontal equations of motion are written separately; the hydrostatic approximation and the continuity equations are rearranged to yield diagnostic equations for π and w, respectively and the governing equations are shown in Table 3.

3. Terrain-related coordinate system

In order to derive the model equation in the terrain-related coordinate system, we make use of the transformed vertical coordinate, namely,

$$z^* = \bar{s}\left(\frac{z - z_G}{s - z_G}\right) \qquad (4)$$

where $s\ (x, y, t)$ is the material surface top of the model, $z_G\ (x, y, t)$ is the terrain height and $\bar{s}$ is the initial value of s (Mahrer and Pielke 1975, 1976).

From the Eqn. (4) the partial derivatives of z^* are obtained. Relations between partial derivatives in original coordinate system (x, y, z, t) and those in the transformed system (x', y', z^*, t') are then obtained. It should be noted here that $x=x'$, $y=y'$ and $t=t'$; the primes are required, nevertheless, to distinguish which system is implied when partial derivatives are taken.

Finally, Table 4 gives all the transformed model equations where primes have been dropped for convenience, although the asterix is retained on z.

TABLE 4

Governing equations in terrain—Following coordinate system

$$\frac{\partial u}{\partial t} = -u\frac{\partial u}{\partial x} - v\frac{\partial u}{\partial y} - w^*\frac{\partial u}{\partial z^*} - \theta\frac{\partial \pi}{\partial x} + g\left[\left(\frac{z^*-\bar{s}}{\bar{s}}\right)\frac{\partial z_G}{\partial x} - \frac{z^*}{\bar{s}}\frac{\partial s}{\partial x}\right] + f_3 v - f_2 w + \frac{\partial}{\partial x}\left(K_H\frac{\partial u}{\partial x}\right) + \frac{\partial}{\partial y}\left(K_H\frac{\partial u}{\partial y}\right) + \left(\frac{\bar{s}}{s-z_G}\right)^2\frac{\partial}{\partial z^*}\left(K_z^{(m)}\frac{\partial u}{\partial z^*}\right)$$

$$\frac{\partial v}{\partial t} = -u\frac{\partial v}{\partial x} - v\frac{\partial v}{\partial y} - w^*\frac{\partial v}{\partial z^*} - \theta\frac{\partial \pi}{\partial y} + g\left[\left(\frac{z^*-\bar{s}}{\bar{s}}\right)\frac{\partial z_G}{\partial y} - \frac{z^*}{\bar{s}}\frac{\partial s}{\partial y}\right] - f_3 u + \frac{\partial}{\partial x}\left(K_H\frac{\partial v}{\partial x}\right) + \frac{\partial}{\partial y}\left(K_H\frac{\partial v}{\partial y}\right) + \left(\frac{\bar{s}}{s-z_G}\right)^2\frac{\partial}{\partial z^*}\left(K_z^{(m)}\frac{\partial v}{\partial z^*}\right)$$

$$\frac{\partial \pi}{\partial z} = -\left(\frac{s-z_G}{\bar{s}}\right)\frac{g}{\theta}$$

$$\frac{\partial \theta}{\partial t} = -u\frac{\partial \theta}{\partial x} - v\frac{\partial \theta}{\partial y} - w^*\frac{\partial \theta}{\partial z^*} + \frac{\partial}{\partial x}\left(K_H\frac{\partial \theta}{\partial x}\right) + \frac{\partial}{\partial y}\left(K_H\frac{\partial \theta}{\partial y}\right) + \left(\frac{\bar{s}}{s-z_G}\right)^2\frac{\partial}{\partial z^*}\left(K_z^{(\theta)}\frac{\partial \theta}{\partial z^*}\right)$$

$$\frac{\partial q}{\partial t} = -u\frac{\partial q}{\partial x} - v\frac{\partial q}{\partial y} - w^*\frac{\partial q}{\partial z^*} + \frac{\partial}{\partial x}\left(K_H\frac{\partial q}{\partial x}\right) + \frac{\partial}{\partial y}\left(K_H\frac{\partial q}{\partial y}\right) + \left(\frac{\bar{s}}{s-z_G}\right)^2\frac{\partial}{\partial z^*}\left(K_z^{(q)}\frac{\partial q}{\partial z^*}\right)$$

$$\frac{\partial w^*}{\partial z^*} = -\left(\frac{\partial u}{\partial x} + \frac{\partial v}{\partial y}\right) + \frac{1}{s-z_G}\left(\frac{\partial z_G}{\partial t} + u\frac{\partial z_G}{\partial x} + v\frac{\partial z_G}{\partial y}\right) - \frac{1}{s-z_G}\left(\frac{\partial s}{\partial t} + u\frac{\partial s}{\partial x} + v\frac{\partial s}{\partial y}\right)$$

4. Auxiliary equations and boundary conditions

Table 4 consists of six equations (four prognostic, two diagnostic) in the unknown variables, u, v, w_*, π, θ, q. The terrain-following coordinate system, however, introduced an additional unknown, s. Furthermore, the vertical eddy diffusion coefficient is dependent on z_i, the planetary boundary layer height. Thus equations for s and z_i are required.

The former is obtained by integrating the continuity equation from $z^* = 0$ to $z^* = \bar{s}$, putting $w_*=0$ at top and bottom. The resulting prognostic equation is :

$$\frac{\partial s}{\partial t} = \frac{\partial z_G}{\partial t} - \frac{1}{s}\int_0^{\bar{s}}\left\{\frac{\partial}{\partial x}\left[u\left(s-z_G\right)\right] + \frac{\partial}{\partial y}\left[v\left(s-z_G\right)\right]\right\}dz^* \qquad (5)$$

where the first term is only required during the early stages of model integration as the terrain is growing.

The prognostic equation for the boundary layer height, z_i, follows Deardorff (1974) :

$$\frac{\partial z_i}{\partial t} = -u\frac{\partial z_i}{\partial x} - v\frac{\partial z_i}{\partial y} + w_i + \frac{1\cdot 8\,[w_*^3 + 1\cdot 1\,u_*^3 - 3\cdot 3\,u_*^2 f_3 z_i]}{g\,\frac{z_i^2}{\theta_s}\cdot\frac{\partial \theta^+}{\partial z} + 9w_*^2 + 7\cdot 2\,u_*^2} \qquad (6)$$

where,

$$w_* = \begin{cases} \left(-\frac{g}{\theta s}u_*\,\theta_*\,z_*\right)^{\frac{1}{3}}, & \theta < 0 \\ 0, & \theta > 0 \end{cases} \qquad (7)$$

θ_s is the potential temperature at the surface, $\partial\theta^+/\partial z$ is the potential temperature gradient immediately above the planetary boundary layer and w_i is the synoptic-scale vertical velocity at the top of the planetary boundary layer. The other symbols have their usual definitions.

The hydrostatic equation is integrated downwards from $z^* = s$ in order to obtain π. Thus

values of $\pi\ (t)$ at $z^*=\bar{s}$ are required. These are determined from

$$\pi\ (s, t\ ) = (\ s, 0\ ) - \frac{g}{\bar{\theta}}\ (\ s - \bar{s}) \qquad (8)$$

where $\bar{\theta}$ is the vertical mean potential temperature in the layer between $\bar{s}$ and s.

The value of K_z at the top of the surface layer is given by

$$K_z{}^m\ (h) = \frac{k\, u_*\, h}{\phi_m\ (\zeta)}$$

$$K_z{}^\theta\ (h) = \frac{k\, u_*\, h}{\phi_\theta\ (\zeta)} \qquad (9)$$

$$K_z{}^q\ (h) = \frac{k\, u_*\, h}{\phi_q\ (\zeta)}$$

where, $h = z_i/25$, $\zeta = z_*/L$ and

$$L = \frac{\theta\, u_*{}^2}{k\, g\, \theta_*} \qquad (10)$$

is the Monin-Obukhov length. In equations (9) the dimensionless velocity, temperature and humidity gradients ϕ_m, ϕ_θ, ϕ_q are from Yamamoto and Shimanuki (1966). The value of $K_z\ (z_i)$ is assumed to be 1 cm^2 s^{-1}.

Surface roughness length is taken to be 4 cm over land and $z_0 = 0.032\ u_*{}^2/g$, $z_0 \geqslant 0.0015$ cm over water (Clarke 1970).

The values of u_* and θ_* are determined iteratively from

$$u_* = \frac{k\ (u^2 + v^2)^{\frac{1}{2}}}{G_i\ (\ |\ \zeta\ |\ ) - G_i\ (\ |\ \zeta_0\ |\ )} \qquad (11)$$

$$\theta_* = \frac{k\ [\theta - \theta\ (z_0)]}{G_i\ (\ |\ \zeta\ |\ ) - G_i\ (\ |\ \zeta_0\ |\ )} \qquad (12)$$

where $\zeta_0 = z_0/L$ and G_i is a profile function ($i = 1$, 2 implies unstable and stable stratifications, respectively).

At $z^* = 0$ the boundary conditions are

$u = v = w^* = 0$

$q =$ constant

$\theta =$ { constant over water; specified as a function (Fourier series) of time over land.

At $z^*=\bar{s}$:

$u = u_g$

$v = v_g$

$w^* = 0$

π is determined from Eqn. (8)

$\theta =$ Constant

At the lateral boundaries :

$$w^* = \frac{\partial s}{\partial t} = \frac{\partial \theta}{\partial x} = \frac{\partial q}{\partial x} = \frac{\partial \pi}{\partial x} = 0$$

on x boundaries

$$w^* = \frac{\partial s}{\partial t} = \frac{\partial \theta}{\partial y} = \frac{\partial q}{\partial y} = \frac{\partial \pi}{\partial y} = 0$$

on y boundaries

$$\frac{\partial u}{\partial x} = \frac{\partial v}{\partial x} = 0$$

on x-outflow boundaries

$$\frac{\partial u}{\partial y} = \frac{\partial v}{\partial y} = 0$$

on y-outflow boundaries

$u =$ constant, $v =$ constant on inflow boundaries

For initial conditions, surface values of pressure, temperature and humidity are specified. The geostrophic wind is also specified. The winds are obtained by integrating the system of equations :

$$\frac{\partial u}{\partial t} = f_3\ (v - v_g) + \frac{\partial}{\partial z}\left[\ K_z{}^{(m)}\ \frac{\partial u}{\partial z}\ \right]$$

$$\frac{\partial v}{\partial t} = -f_3\ (u - u_g) + \frac{\partial}{\partial z}\left[\ K_z{}^{(m)}\ \frac{\partial v}{\partial z}\ \right]$$

for six inertial periods.

5. Numerical techniques

The equations are integrated forward in time using a semi-implicit scheme (Richtmyer and Morton 1967; Kwizak and Robert 1971). Upstream finite differencing is employed to approximate horizontal derivatives. The model grid is staggered with u, v and π defined on the grid points, θ and q defined on levels above and below the main grid levels and w defined on main grid levels but at the centres of the squares formed by four grid points. In order to maintain linear computational stability, the u and v equations are evaluated first, the w equation second (along with the equation for the height of the material surface), followed by the equations for θ, q and π.

In order to describe the semi-implicit time integration scheme it is first necessary to examine the method of evaluating vertical eddy diffusion terms. If the u equation in Table 4 is considered, it is seen that the vertical eddy diffusion is given exactly as

$$\left(\frac{\bar{s}}{s - z_G}\right)^2 \frac{\partial}{\partial z^*}\left[\ K_z{}^{(m)}\ \frac{\partial u}{\partial z^*}\ \right]$$

Letting the subscripts j, $j+1$, $j-1$ represent a grid level, the grid level above and the grid level below, respectively and $j+\frac{1}{2}$, $j-\frac{1}{2}$ represent the staggered grid levels immediately above

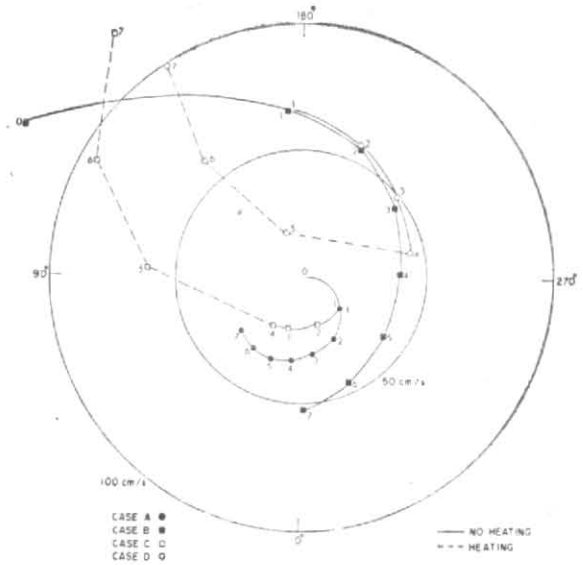

Fig. 1. Hourly vector deviations of wind velocity from equilibrium values over land

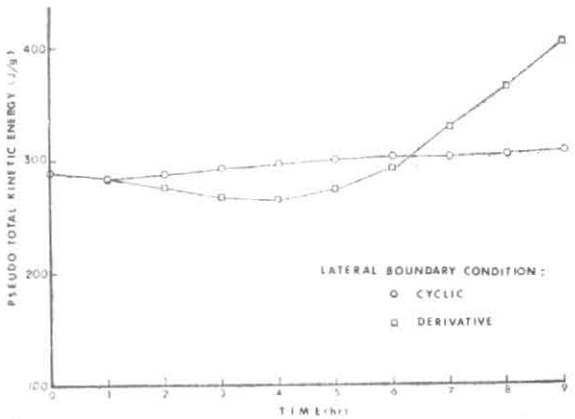

Fig. 2. Pseudo-kinetic energy evolution for analytic ridge case studies with different lateral boundary condition

and below level j on which the eddy coefficients are defined, then the eddy diffusion term is approximated as follows :

$$\left(\frac{\bar{s}}{s-z_G}\right)^2\left(\frac{1}{\triangle z_T}\right)\left[\frac{K_{j+\frac{1}{2}}}{\triangle z_1}\ (u^n{}_{j+1}-u_j{}^{1+n})-\frac{K_{j-\frac{1}{2}}}{\triangle z_2}(u_j{}^{n+1}-u^n{}_{j-1})\ \right]$$

where,

$$\triangle z_T = z^*{}_{j+\frac{1}{2}} - z^*{}_{j-\frac{1}{2}},$$
$$\triangle z_1 = z^*{}_{j+1} - z_j{}^* \ ,$$
$$\triangle z_2 = z^*{}_j - z^*{}_{j-1}$$

and the superscripts n and $n+1$ represent values at the current and subsequent (one time step later) times, respectively.

The presence of the $u_j{}^{n+1}$ values in the right-hand-side of the u equation, makes the scheme for solving this equation implicit. Fortunately, however, the $u_j{}^{n+1}$ term appears in a linear sense and thus it can easily be moved to the left-hand-side of the equation. Mahrer and Pielke (1976) refer to the finite difference representation of the vertical diffusion as a Dufort-Frankel scheme. This is not completely true, although there are similarities (Richtmyer and Morton 1967). The Dufort-Frankel scheme, in fact, uses three time-levels, not two. Nevertheless, the idea of moving the $u_j{}^{n+1}$ term to the left-hand-side is the same as in the Dufort-Frankel scheme. When this is done, the u equation may be expressed in the finite difference form as follows :

$$u_j{}^{n+1} = u_j{}^n + \left[\ \triangle t\left(\frac{\bar{s}}{s-z_G}\right)\left(\frac{1}{\triangle z_t}\right)\times\left(\frac{K_{j+\frac{1}{2}}}{\triangle z_1}\ u^n{}_{j+1}+\frac{K_{j-\frac{1}{2}}}{\triangle z_2}u^n{}_{j-1}\right)+\begin{matrix}\text{other}\\ \text{terms}\end{matrix}\ \right]\Big/\left[\ 1+\triangle t\left(\frac{\bar{s}}{s\ \ z_G}\right)^2\frac{1}{\triangle z_t}\left(\frac{K_{j+\frac{1}{2}}}{\triangle z_1}+\frac{K_{j-\frac{1}{2}}}{\triangle z_2}\right)\right] \tag{14}$$

where the second term in the denominator originated from the $u_j{}^{n+1}$ terms in the diffusion term. The v, θ, and q equations are treated in a similar manner.

The topography is allowed to grow linearly with time during the first 30 minutes of model integration. This technique helps to avoid numerical instabilities. Thereafter a further 3.5-hr of integration are carried out in order to allow the model to approach a steady-state before actual experiments are begun. In our simulation experiments, 11 vertical levels (50, 100, 300, 600, 1000, 1400, 2100, 3000, 4000, 5000, 6000 m) were employed. The horizontal grid spacing was 5 km with 18 grid points in the direction cross-wind to the geostrophic wind and 15 grid points in the longitudinal direction with an additional 3 grid points at each longitudinal boundary spaced 10, 15 and 20 km apart, respectively.

6. Development and tests of the model

The model described above was made available to the author in 1976 in a form coded for

the computer at the National Center for Atmospheric Research (NCAR). The version of the model obtained had not been extensively tested, although it was a refinement of previous model versions. The first task was to modify the code to operate the model on CDC7600 computer facility available to the author at the Atmospheric Environment Service of Canada. The NCAR version, because of the special features of that machine, did not initially run on the AES machine. Different formats for disk-core fast data transfers proved to be the major concern. Initial tests of the model uncovered a number of errors and inconsistencies. Considerable effort was expended in improving the efficiency and generality of the coding. In particular maximum advantage was made of the CDC's directly addressable Large Core Memory not available at NCAR. This resulted in a 40 per cent saving in execution time. After implementing these improvements, using a $20\times18\times11$ grid, each timestep occupied 0.81 seconds of computer time or about 2 minutes for each simulated hour.

6.1. *Initialization*

This model employs an observed vertical mass distribution and specified geostrophic and thermal winds for initialization. The boundary layer initial winds are derived from the prognostic Ekman Eqn. (13) applied over a water surface. However, for simulations over a primarily land surface it is inappropriate to initialize with water roughness. Where the surface roughness and wind profile are incompatible the wind solution evolves through damped inertial oscillations as evident for the case B in Fig. 1. This should be compared with the evolution for case A in which the initialization roughness is compatible with the underlying value. The small residual oscillation for case A is the result of incomplete convergence of the initialization and imposed inhomogeniety in surface characteristics.

Fig. 1 shows the hour-by-hour evolution of wind at the first grid point above the surface for heated and unheated cases with different initializations. The polar plot is of the wind vector deviations from the unheated equilibrium value. Heating for cases C and D commences at hour four. Small discrepancies between heated and unheated cases with a similar initialization is noted because of a slightly altered upper boundary stability imposed. The important point to note is that the two heated cases with different initialization follow similar evolutions after hour four, quite distinct from the evolution of the unheated cases. Based on these considerations an initialization scheme was adopted where wind was initialized to be in Ekman balance with the underlying surface and then the equations integrated forward for a few hours to permit adjustments to advective effects.

6.2. *Boundary conditions*

Difficulties were encountered with the u and v boundary conditions in the early experiments with the model. The problems occurred when a double flow reversal occurred at the boundary in such a way that first inflow, then outflow, then inflow conditions prevailed during the course of the time integration. In the first phase, boundary conditions remained fixed at their initial values. After the first flow reversal, outflow conditions existed and the values of u and v were allowed to change with time in accordance with the zero-derivative condition. Conditions at the boundaries could, therefore, deviate significantly from synoptic values without having harmful effects on the model interior. As soon as a second flow reversal took place, however, the boundary conditions were again fixed, not at initial synoptic values but at the last values attained during the outflow phase. Thus unrealistic values were advected into the model domain from the boundary, causing very rapid degradation of the solution. In order to avoid this problem a temporary solution of applying the zero-derivative condition for u and v at all lateral boundaries regardless of flow direction was implemented.

After examination of results from an idealized ridge experiment, however, it was realized that the zero-derivative condition was not satisfactory. In this experiment an analytic "Witch of Agnesi" ridge of height 100 m, width 30 km at half-height, aligned in a direction perpendicular to the geostrophic wind, was investigated. The airflow was initially in balance over uniform terrain with a neutral temperature stratification and geostrophic wind speed of 10 ms^{-1}. The ridge was allowed to grow to its full height during the first 30 min of integration. A timestep of 30 sec was employed, although tests with a 20 sec timestep indicated no significant change in the results. No surface heating was incorporated, so the surface potential temperature was held constant.

Fig. 2 displays the evolution of pseudo-total kinetic energy (the sum of the squares of the horizontal wind speed at all grid points). During the first six hours of integration with the zero-derivative condition, the kinetic energy remained within 10 per cent of its initial value (despite the effects of terrain-growing). Thereafter it increased rapidly so that after nine hours it was about 38 per cent larger than its initial value. It is evident that the model results were very gradually becoming unrealistic. Wind speeds, for example, attained values near geostrophic over most of the domain (the pseudo-total kinetic energy for a uniform wind speed of 10 ms^{-1} would be approximately 420 J/g, just slightly more than the actual value reached at hour nine).

Further tests of the boundary conditions for the same idealized ridge topography were evidently required. It was felt with this particular

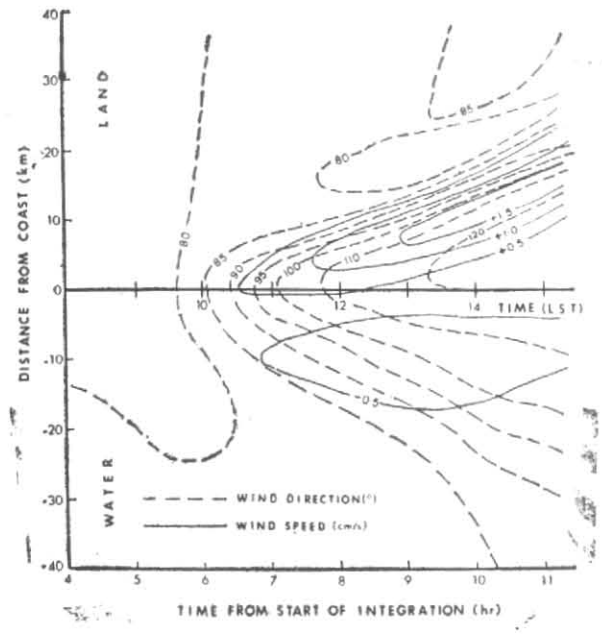

Fig. 3. Evolution of wind direction and vertical wind speed at 50 m for the sea breeze experiment

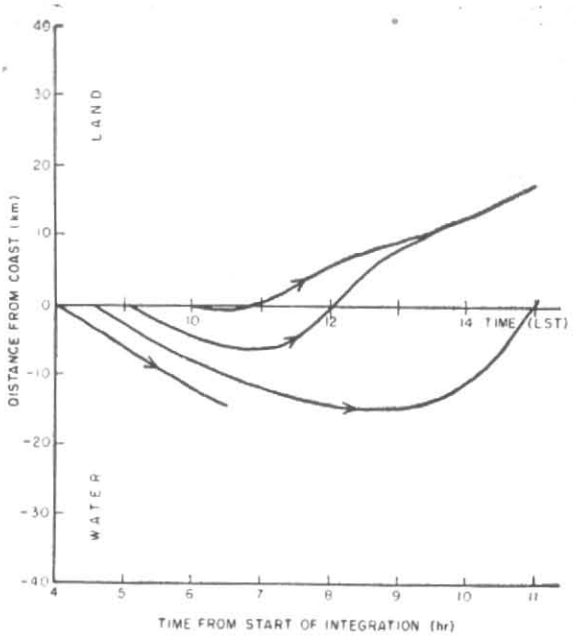

Fig. 4. Pollution trajectories for the sea breeze experiment

terrain that the longitudinal boundaries (upwind and downwind with respect to the geostrophic wind) should not present difficulties since the terrain height gradually approached zero there. Accordingly, the longitudinal boundary conditions were restored to their original state. At the lateral boundaries, on the other hand, the terrain, rising to a maximum of 100 m, extended right to the boundaries. This seemed to be a likely source of difficulties. Hence it was decided to run an experiment with the ridge effectively extending to infinity in both directions. This was accomplished by applying periodic or cyclic boundary conditions on the lateral boundaries. The results of this experiment, also shown in Fig. 2, are much more satisfactory, at least in terms of the pseudo-total kinetic energy which at nine hours is only about 5 per cent greater than its initial value.

It may be concluded from the experiments described above that considerable attention must be drawn to the boundary conditions, particularly in cases where topographic features are close to the boundaries. Additionally, the terrain features may have to be considerably damped near the boundaries.

6.3. *Idealized sea breeze experiment*

A numerical experiment was performed with the model in order to simulate an idealized coastal situation. A straight coastline approximately through the middle of the model domain was specified to be aligned to the geostrophic wind. The land was assumed to have zero elevation everywhere and was located to the right with respect to the geostrophic wind direction. The geostrophic flow was assumed to be easterly (90°), the land was to the north of an east-west shoreline and initial wind directions at the lowest grid level (50 m) were approximately 80°. Heating was begun after four hours of integration (at 8 a.m. I.S.T.) having an amplitude of 6°C which is reached approximately 8-9 hours after the commencement of heating.

Wind direction and vertical wind speed results are shown in Fig. 3. The time scale on the abscissa begins at the time of commencement of heating, 4 hours after the start of integration or at an assumed time of 8 a.m. I.S.T. The sea breeze begins at about 10.20 a.m., the wind direction continuing to shift thereafter until between 1.00 and 2.00 p.m. a direction of about 120° is achieved. This shift represents a veer of more than 40° from the equilibrium unheated situation. These wind direction changes are accompanied by weak subsidence over the water and somewhat stronger upward vertical motion over the land, reaching a maximum in excess of 1.5 cm s^{-1} at about 2.30 p.m. This experiment was terminated at 3 p.m., approximately 1.5 hours before the time of maximum surface temperature. During the period of simulation, however, the sea breeze was seen to penetrate inland about 20 km against an adverse equilibrium unheated surface flow oriented at more than 10° to the shoreline.

This sea breeze case study illustrates that the model is capable of reasonably simulating the atmospheric flow phenomena. In the following the implications of this case study to air quality prediction are investigated.

7. Application to air quality studies

Here mesoscale air pollution trajectories for a simple sea breeze simulation discussed previously are calculated. This study illustrates how even a simple simulation can lead to important insights regarding the role of mesoscale processes in air pollution dispersion.

An air pollution trajectory is the path followed by the average particle released from a particular point at a particular time and constrained to move with the wind. Computer models produce values of wind at discrete points and times. Calculation of trajectories relies on interpolating winds so produced and moving a particle to follow the wind at that point. In our calculations the interpolation was performed using a spline-under-tension. Because of the spatial symmetry of the particular problem studied here a simple two-dimensional (one spatial and one temporal) routine was employed, the NCAR Scientific Subroutine Package "SURF".

The flow solution for the heated coastal situation is employed to drive the trajectory model. Since the situation lacks any variation in the x (along the geostrophic wind) direction only one column normal to the coastline is considered at any one time. Further, since we are primarily interested in low level trajectories, which is where pollution is emitted, vertical motions are neglected. Fig. 3 shows that vertical velocities are quite weak over land for this situation prior to about 11.30 a.m. and over the water for most of the period. Thus we can expect that results for trajectories would be misleading over land after 11.30 a.m. The trajectories calculated are shown in Fig. 4. Trajectory origins 1/2 km inland from the coast at 8 a.m., 8.30 a.m., 9 a.m. and 10 a.m. are considered.

Trajectories starting at times upto 8 a.m. proceed slowly offshore, failing to be markedly influenced by the sea breeze circulation by the end of the time period. Only the initial portion of the trajectory is shown. The trajectory starting at 8.30 a.m. proceeds off-shore under the prevailing flow, but is overtaken by the sea breeze effect and turns back toward land at 1.45 p.m. making a landfall just before 3.00 p.m. This is a long over-water trajectory so that deposition mechanisms would have a chance to deplete pollutant but it should be noticed that the trajectory is under subsiding motion for most of its length suggesting that vertical dispersion would be suppressed. Only one-half hour later a trajectory started from the same location moves out over the water only about 6 km before doubling back toward land, crossing the coast near noon. It is interesting that the 8.30 a.m. and 9.00 a.m. trajectories return to the coast three hours apart, but onshore wind speeds are still significant during this three hour period. The trajectory starting at 10.00 a.m. moves along the coast as the sea breeze sets in for nearly one hour before moving inland. If the coastal strip is a high pollutant source region, as is often the case, this trajectory coupled with destabilisation leading to fumigation will result in high ambient air pollution levels.

To summarize the pollution conditions inland of a coastal strip pollution source, the temporal variation seems fairly complex. Prior to the onset of the sea breeze the pollutant emitted is advected out over the sea and inland pollution levels are at background. As the sea breeze sets in high ambient air pollution levels are to be expected due to along coast air trajectories. Up until one and half-hours after this ambient pollution level should gradually decrease as each air parcel effectively gets a double dose of pollutant, but the first dose moves progressively further "upwind". The hours between noon and 3.00 p.m. should see improved air quality as subsident air from aloft over the water feeds inland. However, it may be that some of this has been cycled through sea breeze direct circulation and thus contains pollutant. After 3.00 p.m., largely "double dose pollutant" air will again be crossing the coast, but its over-water trajectory is rather long so that air quality would only likely be moderately elevated above that for completely clean air crossing the coast.

8. Conclusions

The foregoing study illustrates the potential for mesoscale modelling in air quality studies. The Pielke model, as discussed herein, has certain limitations for air quality purposes but can still provide a rapid means to gather valuable qualitative understanding of specific classes of pollutant transport situations. This capibility is demonstrated in the coastal pollution trajectory study. The real potential of such modelling must rest on inclusion of sub-grid scale motions integrated with explicitly modelled motions to predict turbulent dispersion. It is hoped that three dimensional trajectories (one horizontal, one vertical and one temporal dimension) would provide further insight particularly with respect to the impact on air quality of subsiding air over the coastal waters.

Acknowledgements

The computer facilities for this study was provided by the Atmospheric Environment Service, Canada which is gratefully acknowledged. Dr. R.A. Pielke of the University of Virginia kindly provided a computer list of his model and gave permission to obtain a copy of the model from NCAR.

References

Busch, N.E., 1973, *On tne mechanics of atmospheric turbulence, Workshop on Micrometeorlogy,* D.A. Haugen (Ed.), Am. Met. Soc., Boston, pp. 1-65.

Clarke, R.H., 1970, Recommended methods for the treatment of the boundary layer in numerical models, *Austr. Met. Mag.*, **18,** 51-73.

Deardorff, J.W., 1974, Three-dimensional numerical modelling of the planetary boundary layer, *Bound. Layer Met.*, **7,** 81-106.

Haltiner, G.J., 1971, *Numerical Weather Predictions,* Wiley, New York, 317 pp.

Mahrer, Y. and Pielke, R., 1975, A numerical study of the airflow over mountains using the two-dimensional version of the University of Virginia Mesoscale Model, *J. atmos. Sci.*, **32,** 2144-2155.

Mahrer, Y. and Pielke, R., 1976, Numerical simulation of the airflow over Barbados (Communicated).

Monin, A.S. and Yaglom, A.M., 1971, *Statistical Fluid Mechanics, Mechanics of turbulance :* 1, MIT Press, Cambridge, Mass., 769 pp.

Phillips, N.A., 1957, A coordinate system having some special advantages for numerical forecasting, *J. Met.*, **14,** 184-185.

Pielke, R.A., 1973, A three-dimensional numerical model of the sea-breezes over south Florida, Ph. D. dissertation, The Pennsylvannia State University, 135 pp.

Pielke, R.A., 1974(a), A three dimensional numerical model of the sea-breeze over south Florida, *Mon. Weath. Rev.*, **102,** 115-139.

Pielke, R.A. 1974(b), A comparison of Three-Dimensional and Two-Dimensional Numerical Predictions of sea-breezes, *J. atmos. Sci.*, **31,** 1577-1585.

Pielke, R.A. and Mahrer, Y., 1975, Representation of the heated planetary boundary layer in mesoscale models with coarse vertical resolution, *J. atmos., Sci.*, **32,** 2288-2308.

Richtmyer, R.D. and Morton, K.W., 1976, *Finite Difference Methods for Initial-Value Problems,* 2nd ed., Interscience Pub., New York.

Yamamoto, G. and Shimamuki, A., 1966, Turbulent transfer in diabatic conditions, *J. met. Soc. Japan,* **44,** 301-307.